

X-Ray Sources in the Star Forming Galaxies NGC 4194 and NGC 7541

Philip Kaaret^{1,2} and Almudena Alonso-Herrero³

ABSTRACT

We examine the X-ray point source population and 2-10 keV luminosity for two galaxies with high star formation rates (SFRs), NGC 4194 and NGC 7541. The X-ray point source luminosity function (XLF) for these two galaxies is consistent with the XLF found by Grimm et al. (2003) for a sample of star-forming galaxies. Combining our results with a sample of galaxies with SFRs above $1 M_{\odot}/\text{yr}$, we find that the number of X-ray point sources above a luminosity of $2 \times 10^{38} \text{ erg s}^{-1}$ is $N = (1.8 \pm 0.4) \text{SFR}/(M_{\odot} \text{ yr}^{-1})$. This number is lower than previously inferred by Grimm et al. based on a sample of galaxies with lower SFRs. We find that the ratio of X-ray luminosity in the 2-10 keV band to SFR is $L_X/(10^{40} \text{ erg s}^{-1}) = (0.37 \pm 0.08) \text{SFR}/(M_{\odot} \text{ yr}^{-1})$. This value may serve as a calibration in attempts to use X-ray luminosity to measure the SFR of galaxies at cosmological distances. The ratio of mass accreted onto compact objects versus mass used to form stars is near 10^{-6} . This ratio may be useful in constraining population synthesis models of X-ray binary formation in actively star forming systems.

Subject headings: black hole physics – galaxies: individual: NGC 4194 – galaxies: individual: M100 – galaxies: individual: NGC 4945 – galaxies: individual: NGC 7541 – galaxies: stellar content – X-rays: galaxies

1. Introduction

The bulk of bright X-ray sources in most galaxies are compact objects formed at the endpoint of the stellar evolution of massive stars (typically $> 8M_{\odot}$). Because compact objects can be visible as X-ray binaries for lifetimes far exceeding those of their progenitor massive stars, the X-ray binary populations may be used as ‘fossils’ to study the star formation history of their host galaxies (Griffiths & Padovani 1990; David et al. 1992). Recently, Ranalli et al. (2003) demonstrated a correlation between the 2-10 keV X-ray luminosity and star formation rates (SFR) for 23, mainly nearby, galaxies.

Grimm et al. (2003), hereafter GGS03, extended these results to consider the X-ray point source luminosity function (XLF) in addition to the total X-ray luminosity. They found a correlation between the number of X-ray sources in a galaxy and the star formation rate. This correlation does not suffer the strong Malmquist bias of the luminosity correlation. However, due to the limitations of their sample, GGS03 measured the correlation between the number of X-ray sources in a galaxy and the star formation rate only for galaxies with star formation rates of $7M_{\odot}/\text{yr}$ or less. It is of interest to extend these measurements to galaxies with larger star formation rates.

We have obtained *Chandra* observations of two galaxies, NGC 4194 and NGC 7541, selected from the sample of Devereux (1989). Both have high star formation rates, near $12M_{\odot}/\text{yr}$, but are close enough, nearer than 40 Mpc, to distinguish individual X-ray sources. See Table 1 for some basic properties of the galaxies. NGC 4914, also known as the Medusa, is a minor merger at a distance

¹Department of Physics and Astronomy, University of Iowa, Van Allen Hall, Iowa City, IA 52242, USA

²Université Paris 7 Denis Diderot and Service d’Astrophysique, UMR AIM, CEA Saclay, F-91191 Gif sur Yvette, France

³Departamento de Astrofísica Molecular e Infrarroja, Instituto de Estructura de la Materia, CSIC, E-28006 Madrid, Spain

Name	NGC 4194	NGC 7541
RA (J2000)	12 14 09.6	23 14 43.86
DEC (J2000)	+54 31 35.8	+04 32 01.8
Distance (Mpc)	39.5	37.1
SFR (M_{\odot}/yr)	12.3	12.0
Major diameter	1.82'	3.47'
Minor diameter	1.10'	1.15'
Position angle	164°	102°
X-ray sources	5-10	15
$L_X(10^{40} \text{ erg s}^{-1})$	3.0	1.8

Table 1: contains for each galaxy: the galaxy name, RA, DEC, distance, star formation rate (SFR), the major and minor diameters and position angle of the d_{25} ellipse from the RC3 catalog, the number of X-ray sources above a luminosity of $2 \times 10^{38} \text{ erg s}^{-1}$, and the total X-ray luminosity (L_X) in the 2-10 keV band. The distances are from Weistrop et al. (2004) for NGC 4914 and from Jha et al. (2007) for NGC 7541.

of 39.5 Mpc (Weistrop et al. 2004). NGC 7541 is an SBc galaxy and has a companion galaxy NGC 7537. It was the host of SN1998dh which allows an accurate distance estimate of 37.1 ± 1.5 Mpc (Jha et al. 2007). We also extracted results from the literature and from the data archives for additional galaxies with star formation rates above $1 M_{\odot}/\text{yr}$. Our observations and analysis are described in section §2. In §3, we discuss the X-ray point source luminosity functions. In §4, we discuss the relation of X-ray source populations to star formation rate.

2. Observations and Analysis

2.1. New observations

Observations of NGC 4194 and NGC 7541 were made using the Advanced CCD Imaging Spectrometer (ACIS; Bautz et al. 1998) on board the Chandra X-Ray Observatory. The *Chandra* observation of NGC 4194 (ObsID 7071) began on 9 September 2006 at 23:30:18 UT and had a useful exposure of 35.5 ks. The observation of NGC 7541 (ObsID 7070) began on 31 October 2006 at 21:35:08 UT and had a useful exposure of 39.0 ks. The Chandra data were subjected to standard data processing and event screening. The total rate on the S3 chip was below 1.5 c/s for NGC

4194 and below 1.6 c/s for NGC 7541 indicating that there were no strong background flares.

For each observation, we constructed an image using all valid events in the 0.3–8 keV band on the S3 chip and used the *wavdetect* tool which is part of the *CIAO* version 3.4 data analysis package to search for X-ray sources. For NGC 4194, which has extended diffuse X-ray emission near its core, we also searched for sources in the 1.5–8 keV band. Lists of sources with detection significance of 3.0σ or higher within the d_{25} ellipse of each galaxy are given in Tables 2 and 3. In order to calculate the source fluxes, we computed an exposure map for an assumed source spectrum of a powerlaw with photon index of 1.7 absorbed by the total Galactic H I column density along the line of sight (Dickey & Lockman 1990) which we take as $5.2 \times 10^{20} \text{ cm}^{-2}$ for NGC 4194 and $1.5 \times 10^{20} \text{ cm}^{-2}$ for NGC 7541. We also calculated source luminosities in the 2-10 keV band using the same spectral model and assuming that the sources are at the same distance as the galaxy. In order to give some indication of the spectral shape of each source, we calculate the ratio of the Chandra counts in the 1–8 keV band to counts in the 0.3–8 keV band. The source fluxes, luminosities, and colors are listed in Tables 2 and 3.

We searched for counterparts to the X-ray sources in the USNO B1 catalog (Monet et al. 2003) to attempt to improve the *Chandra* astrometry. We found three matches within $1''$ in the S3 image for NGC 4194. After a shift of $0.3''$, the X-ray and optical positions for all three objects agree within $0.22''$. For NGC 7541, we found two coincidences, but both were at the edge of the S3 chip where the *Chandra* point spread function is relatively large and the source location accuracy is relatively poor. Thus, we chose not to correct the astrometry for NGC 7541. We also searched for counterparts in the 2MASS catalog (Skrutskie et al. 2006). The only counterpart in the NGC 4194 field was for the nucleus of the galaxy. The core of NGC 4194 has strong, extended near-IR emission which may obscure point sources near the center of the galaxy. There were several counterparts within $1''$ within NGC 7541, but crowding of 2MASS sources in the disk of the galaxy prevents confident assignment of unique counterparts.

We searched for X-ray variability by comparing

TABLE 2
X-RAY SOURCES WITHIN THE FIELD OF NGC 4194

#	RA	DEC	S/N	Counts	Flux (10^{-15} erg cm $^{-2}$ s $^{-1}$)	Luminosity (10^{38} erg s $^{-1}$)	Hardness	Counterpart
1	12 14 09.69	+54 32 15.6	164.8	455	110 ± 5	129	0.54	Nucleus SDSS
2	12 14 09.62	+54 31 35.9	139.8	870	210 ± 7	246	0.68	
3	12 14 06.18	+54 31 43.0	126.2	390	95 ± 5	111	0.60	
4	12 14 09.99	+54 31 27.1	13.3	86	22 ± 2	25.5	0.48	
5	12 14 09.90	+54 31 42.2	5.6	21	5.1 ± 1.1	5.9	0.95	
6	12 14 09.23	+54 31 44.9	4.7	21	5.1 ± 1.1	5.9	0.52	

NOTE.—isted for each source: number; RA and DEC – the position of the source in J2000 coordinates; S/N – significance of the source detection as calculated by *wavdetect*; Counts - counts in the 0.3–8 keV band; Flux – source flux in units of 10^{-15} erg cm $^{-2}$ s $^{-1}$ in the 0.3–8 keV band calculated assuming a power law spectrum with photon index of 1.7 and corrected for the Galactic absorption column density along the line of sight; Luminosity – source luminosity in units of 10^{38} erg s $^{-1}$ in the 2–10 keV band using the same spectral model; Hardness - the hardness ratio defined as the ratio of counts in the 1–8 keV band to counts in the 0.3–8 keV band.

TABLE 3
X-RAY SOURCES WITHIN THE FIELD OF NGC 7541

#	RA	DEC	S/N	Counts	Flux (10^{-15} erg cm $^{-2}$ s $^{-1}$)	Luminosity (10^{38} erg s $^{-1}$)	Hardness	Counterpart
1	23 14 42.21	+04 31 40.1	71.0	229	49 ± 3	57.0	0.73	2MASS
2	23 14 42.39	+04 32 31.0	44.7	121	26 ± 2	30.3	0.73	
3	23 14 38.85	+04 32 04.1	23.0	63	13.6 ± 1.7	15.8	0.73	
4	23 14 43.91	+04 32 02.6	22.3	141	30 ± 3	35.1	0.60	
5	23 14 39.17	+04 32 04.3	20.4	50	10.8 ± 1.5	12.5	0.80	
6	23 14 39.81	+04 32 18.2	19.3	46	9.9 ± 1.5	11.6	0.96	
7	23 14 46.22	+04 31 56.4	14.9	48	10.3 ± 1.5	12.0	0.83	
8	23 14 39.92	+04 32 02.0	13.9	39	8.4 ± 1.3	9.7	0.62	
9	23 14 46.01	+04 32 03.2	11.4	36	7.7 ± 1.3	9.0	0.89	
10	23 14 46.97	+04 31 54.2	8.3	21	4.5 ± 1.0	5.2	0.76	
11	23 14 42.63	+04 32 15.7	6.5	18	3.9 ± 0.9	4.5	0.78	
12	23 14 40.21	+04 32 03.9	5.8	14	3.0 ± 0.8	3.5	1.00	
13	23 14 42.43	+04 32 03.4	4.7	13	2.8 ± 0.8	3.2	0.77	
14	23 14 47.33	+04 32 06.4	4.6	10	2.2 ± 0.7	2.5	0.80	
15	23 14 41.64	+04 31 51.7	3.4	8	1.7 ± 0.6	2.0	0.88	

NOTE.—The quantities are as defined for Table 2.

the photon arrival times for each source to the distribution expected for a constant source with the same average flux using a Kolmogorov-Smirnoff (KS) test. No background subtraction was performed. We find significant variability only for CXOU J231438.85+043204.1 in NGC 7541. This source shows a marked decrease in flux across the observation.

We performed X-ray spectral fitting for the sources with more than 100 counts. We fitted the spectra using the *Sherpa* fitting package and response matrices calculated using the *mkrmf* tool in *CIAO*. We used the χ^2 -Gehrels statistic to evaluate the quality of the fits due to the low numbers of counts. The fit results are shown in Table 4. All of the spectra, except for the nuclear region of NGC 4194, were adequately fitted with an absorbed power-law. NGC 4194 shows extended X-ray emission near the nucleus, so we extracted two spectra: one in a circular region with a radius of 2 pixels and the other with a radius of 13 pixels covering the region of extended emission. We fit these spectra with a model consisting of a power-law plus thermal emission from diffuse gas, specifically the APEC model. The large region spectrum is best fitted, $\chi^2/\text{DoF} = 54.3/99$, when the thermal component has a temperature $kT = 0.77 \pm 0.06$ keV and an unabsorbed flux of $(9.7 \pm 1.8) \times 10^{-14} \text{ erg cm}^{-2} \text{ s}^{-1}$ in the 0.3–8 keV band, the power-law component has a flux of $(2.3 \pm 0.6) \times 10^{-13} \text{ erg cm}^{-2} \text{ s}^{-1}$ and a photon index $\Gamma = 2.0 \pm 0.3$, and the absorption column density is $N_H = (1.3 \pm 0.5) \times 10^{21} \text{ cm}^{-2}$. We fitted the small region spectrum with the APEC temperature fixed to $kT = 0.77$. In the best fit, $\chi^2/\text{DoF} = 22.0/33$, the power-law component describing the nuclear point source had a photon index $\Gamma = 1.7 \pm 0.4$ and an unabsorbed flux of $(9 \pm 3) \times 10^{-14} \text{ erg cm}^{-2} \text{ s}^{-1}$ in the 0.3–8 keV band where we have corrected for the encircled energy within the 2 pixel radius.

Observations of both galaxies were made using the Advanced Camera for Surveys (ACS) on the Hubble Space Telescope (HST) under GO program 10769. Images were obtained in the broad band filter F814W (I-band) using the Wide-Field Camera (WFC). NGC 7541 was observed on 8 August 2006. We used the images delivered by the standard ACS pipeline processing (OPUS 2006.5 and CALACS code version 4.6.1) which removes cosmic-rays, corrects for optical distortion, and

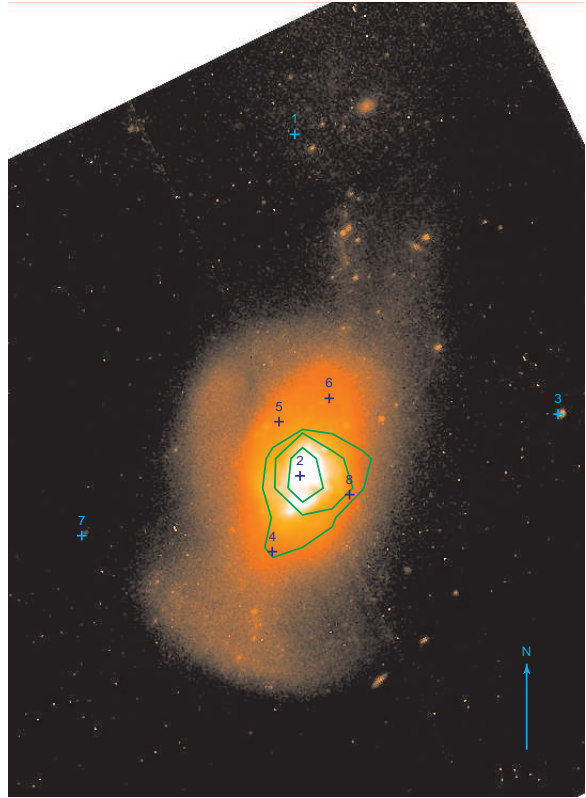


Fig. 2.— NICMOS F110W infrared image of NGC 4194. The green contours represent the diffuse X-ray emission and correspond to 0.5, 1, and 2 counts per ACIS pixel ($0.492''$ square). The diffuse X-ray emission is located at the region with a dense stellar population as indicated by the IR intensity. The crosses indicate the positions of the X-ray sources listed in Table 2. The arrow points North and has a length of $10''$.

dither combines the images. We aligned the image to stars in the USNO B1.0 catalog (Monet et al. 2003) using the Graphical Astronomy and Image Analysis Tool (*GAIA*; Starlink version 2.8-0). Fig. 1 shows the positions of the X-ray sources detected with Chandra overlaid on the HST/ACS I-band image of NGC 7541.

Observations of both galaxies were also made with the Near Infrared Camera and Multi-Object Spectrometer (NICMOS) on HST using the NIC3 camera that has a pixel size of $0.2''$ and a field of view (FOV) of $\sim 51.2'' \times 51.2''$. We used two broad-band filters: F110W and F160W. The images were reduced using the *HST/NICMOS*

TABLE 4
X-RAY SPECTRA FOR BRIGHT POINT SOURCES

RA	DEC	χ^2/DoF	Γ	N_H (10^{21} cm^{-2})	Flux ($10^{-14} \text{ erg cm}^{-2} \text{ s}^{-1}$)
NGC 4194					
12 14 09.69	54 32 15.6	18.2/36	$2.6^{+0.5}_{-0.4}$	$1.1^{+0.9}_{-0.6}$	6.1
12 14 06.18	54 31 43.0	10.5/33	$2.1^{+0.5}_{-0.4}$	$0.6^{+0.8}_{-0.1}$	6.3
NGC 7541					
23 14 42.21	04 31 40.1	13.8/19	$2.2^{+0.6}_{-0.5}$	$2.6^{+1.6}_{-1.2}$	3.3
23 14 42.39	04 32 31.0	2.3/12	$2.0^{+0.9}_{-0.7}$	$2.0^{+2.2}_{-1.8}$	2.1
23 14 43.91	04 32 02.6	8.1/11	$2.3^{+1.3}_{-0.9}$	$1.8^{+2.6}_{-1.6}$	1.5

NOTE.—isted for each source: the position in RA and DEC (J2000), the goodness of the fit, the photon index, the absorption column density, and the absorbed flux in the 0.3–8 keV band.

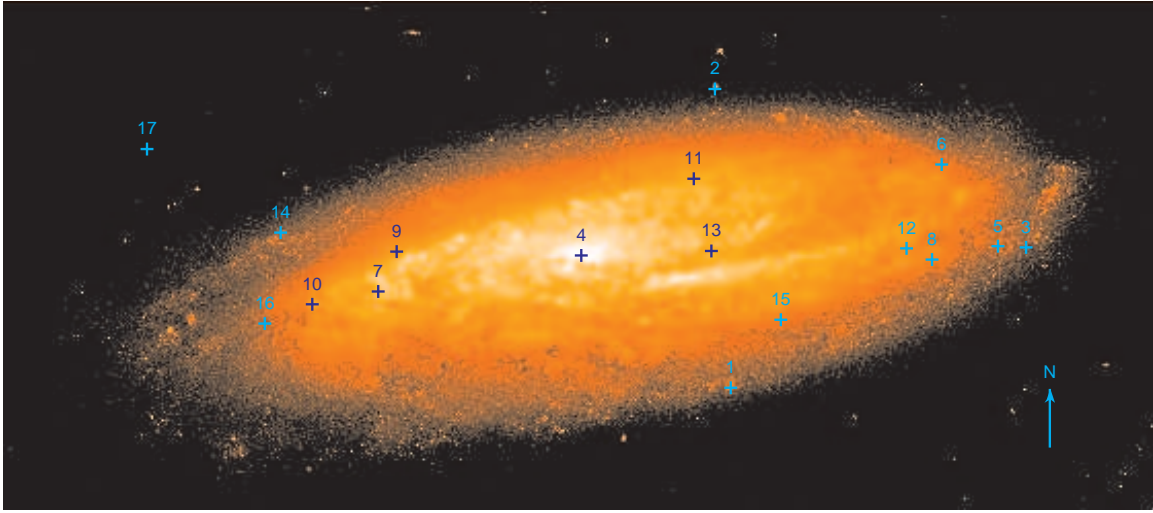


Fig. 1.— HST/ACS F814W (I-band) image of NGC 7541. The crosses indicate the positions of the X-ray sources listed in Table 3. The arrow points North and has a length of $10''$.

pipeline routines, which involve subtraction of the first readout, dark current subtraction on a readout-by-readout basis, correction for linearity and cosmic ray rejection, and flat fielding. Since the size of the galaxies exceeds the FOV of the NIC3 camera, for each galaxy we took four pointings to produce a final mosaic covering an approximate FOV of $1.6' \times 1.6'$. We aligned the mosaic images to stars in the 2mass catalog (Skrutskie et al. 2006) using *GAIA*. Fig. 2 shows the positions of the X-ray sources and contours of the X-ray diffuse emission overlaid on the F110W mosaic of NGC 4194.

One of the sources in the NGC 4194 field with

an USNO B1 counterpart falls within the d_{25} ellipse of the galaxy. The R magnitude is 19.43. The X-ray to optical flux ratio of the source, $\log(f_x/f_R) = \log f_X + 5.50 + R/2.5 = 0.9$, is in the range found for AGN (Hornschemeier et al. 2001). This source also has a Sloan Digital Sky Survey counterpart, SDSS J121406.21+543143.1, which is identified as a faint quasar based on the optical colors. The source lies within the d_{25} ellipse of NGC 4194, but not in the main body of the galaxy or the tidal tail. On the HST F814W (I-band) image, we find no stars close to the source other than the counterpart. Thus, we conclude that the source is most likely a background AGN.

Galaxy	Distance (Mpc)	SFR (M_{\odot}/yr)	Sources
NGC 4194	39.5	12.3	10
NGC 7541	37.1	12.0	15
NGC 1068	14.4	9.0	18
M51	8.4	4.9	13
Antennae	13.8	3.6	9
M100	16.8	3.3	11
NGC 4945	3.7	2.7	4
M82	3.6	1.4	7
NGC 4579	16.8	1.3	3
M74	8.8	1.2	2

Table 5: contains for each galaxy: the galaxy name, distance, star formation rate, and net number of X-ray sources above a luminosity of $2 \times 10^{38} \text{ erg s}^{-1}$ in the 2-10 keV band after removal or subtraction of background AGN.

2.2. Additional galaxies

We analyzed archival Chandra data for the galaxies M100 and NGC 4945 following the same procedures described above. The observation of NGC 4945 was made on 27 Jan 2000 (ObsID 864) beginning at 19:00:10 UT with an exposure of 24.5 ks. We reprocessed the data using recent calibrations and procedures current in Ciao 3.4. The galaxy is larger than the ACIS S3 chip, but the roll angle of the observation placed the entire D_{25} ellipse of the galaxy on ACIS chips S2, S3, and S4. Thus, we extracted sources and calculated exposure maps for all three chips. The observation of M100 was made on 18 Feb 2006 (ObsID 6727) beginning at 19:00:10 UT with an exposure of 24.5 ks. The target was SN 1979C, which is not at the center of M100, so we included ACIS chips S2 and S3 in order to cover the whole galaxy. Lists of sources with detection significance of 3.0σ or higher within the d_{25} ellipse of each galaxy are given in Tables 6 and 7. We estimated the number of background AGN at fluxes above that equivalent to $2 \times 10^{38} \text{ erg s}^{-1}$ within each galaxy using the source counts from Giacconi et al. (2001) in the 2–10 keV band.

For the galaxies M51, M74, M82, NGC 4579, NGC 1068, and the Antennae, we extracted source counts from the literature. In each case, we estimated the number of background AGN in-

cluded in the count using the source counts from Giacconi et al. (2001) unless this was already done in the reference or background and foreground sources were already excluded by a search for counterparts at other wavelengths. Below we will integrate the XLF to find the total X-ray luminosity due to point sources. For this to be valid, the energy band used to find the point source luminosities must match the energy band used to calculate the total X-ray luminosity, specifically 2–10 keV. Thus, we corrected the source luminosities from the literature to this energy band. We used the spectral model assumed in each paper. However, using a power-law model as for NGC 4194 and NGC 7541 produced no significant change.

We note that GGS03 extracted X-ray point source luminosities from the literature and made no attempt to correct for the differing energy bands and assumptions concerning spectra shape made in the various papers. We find that, for the galaxies in their sample, making the energy band correction produces a large change only for the Antennae. In addition to the energy band correction, Ivo et al. (2004) recently found a distance to the Antennae based on the red giant branch tip of 13.8 ± 1.7 Mpc that is significantly lower than previous distances including that used by GGS03. Also, one of the Antennae sources was identified as a background AGN (Clark et al. 2005). Thus, the star formation rate for the Antennae becomes $3.6 M_{\odot} \text{ yr}^{-1}$ and the number of sources above $2 \times 10^{38} \text{ erg s}^{-1}$ becomes 9.

For M51, we find 11 net sources above $2 \times 10^{38} \text{ erg s}^{-1}$ in the 2-10 keV band using the 2–8 keV band results of Terashima & Wilson (2004). For M74, we estimate two sources from the 2–8 keV band results of Kilgard et al. (2002, 2005). For M82, we estimate 7 net sources from the 2–10 keV band results of Griffiths et al. (2000). For NGC 4579, we estimate 3 sources from the results of Eracleous et al. (2002). For NGC 1068, we estimate 18 net sources from the 0.5–8 keV band results of Smith & Wilson (2003). For these galaxies, we have adopted the SFRs quoted by GGS03 rescaled to the distances listed in Table 5 except for NGC 1068 and NGC 4945 where we have calculated the SFR from the FIR luminosities quoted in Koribalski (1996) rescaled to the distances quoted in Table 5. Both are Seyfert 2 galaxies containing an active galactic nucleus which produces infrared

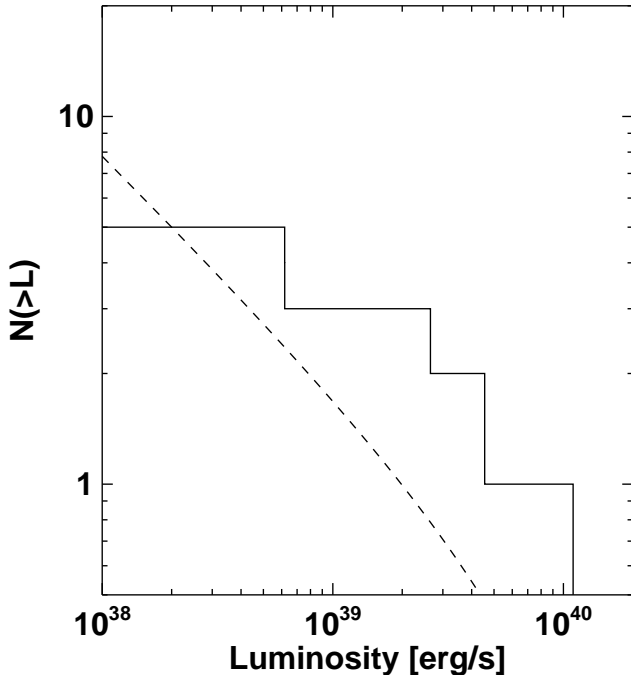


Fig. 3.— X-ray point source luminosity function for NGC 4194. The dashed line indicates the functional form from GGS03 normalized to have the same number of sources with luminosity above $2 \times 10^{38} \text{ erg s}^{-1}$ as observed in the galaxy.

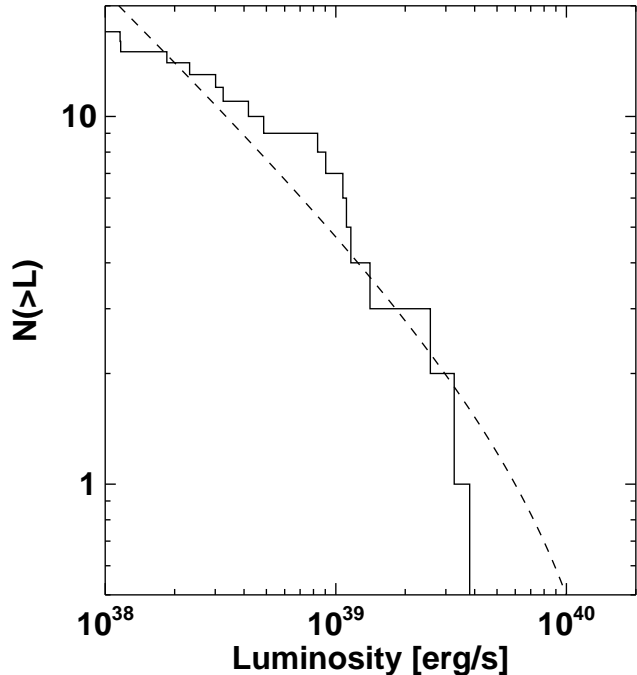


Fig. 4.— X-ray point source luminosity functions for NGC 7541. The dashed line indicates the functional form from GGS03 normalized to have the same number of sources with luminosity above $2 \times 10^{38} \text{ erg s}^{-1}$ as observed in the galaxy.

emission. Thus, the SFR calculated from the total FIR luminosity may overestimate the true SFR. However, the starburst in NGC 1068 is known to dominate the flux at wavelengths longer than $30 \mu\text{m}$ (Telesco et al. 1984), so AGN contamination does not strongly affect the SFR estimate.

3. X-ray point source luminosity functions

Figs. 3 and 4 show the X-ray point source luminosity functions (XLFs) for NGC 7541 and NGC 4194. The dashed curves are the ‘universal’ XLFs for star-forming galaxies suggested by GGS03. The dashed curves are normalized to have the same number of sources with luminosity above $2 \times 10^{38} \text{ erg s}^{-1}$ as observed in the comparison galaxy. A Kolmogorov-Smirnov test indicates that the distributions for both galaxies are consistent with this form.

At low luminosities, $2\text{--}5 \times 10^{38} \text{ erg s}^{-1}$, the XLF for NGC 4194 appears flatter than the GGS03 XLF. The observation duration is sufficient to de-

tect sources with luminosities down to at least $2 \times 10^{38} \text{ erg s}^{-1}$ with high efficiency; a luminosity of $2 \times 10^{38} \text{ erg s}^{-1}$ should produce 7 counts and a 3.2σ detection. However, the diffuse X-ray emission near the nucleus, where most of the star formation is concentrated, hampers our ability to detect sources. Indeed, there is a possible source located at R.A. = $12^{\text{h}}14^{\text{m}}08^{\text{s}}.96$, Decl. = $+54^{\circ}31'33''.7$ (J2000) that lies in the region of diffuse emission. The source is marginally detected at a significance of 2.4σ and only in the 1.5–8 keV band, but appears to have a luminosity of $5 \times 10^{38} \text{ erg s}^{-1}$.

The excess 2–10 keV flux in the nuclear region not accounted for in detected point sources is $5.5 \times 10^{-14} \text{ erg cm}^{-2} \text{ s}^{-1}$ equivalent to a luminosity of $1.0 \times 10^{40} \text{ erg s}^{-1}$. By integrating a differential XLF, we can find the number of sources above a given luminosity. By weighting the integrand by the luminosity, we can find the total luminosity produced by the set of sources above a given luminosity. For the GGS03 XLF, specifically eq. 6 in their paper, the relation between

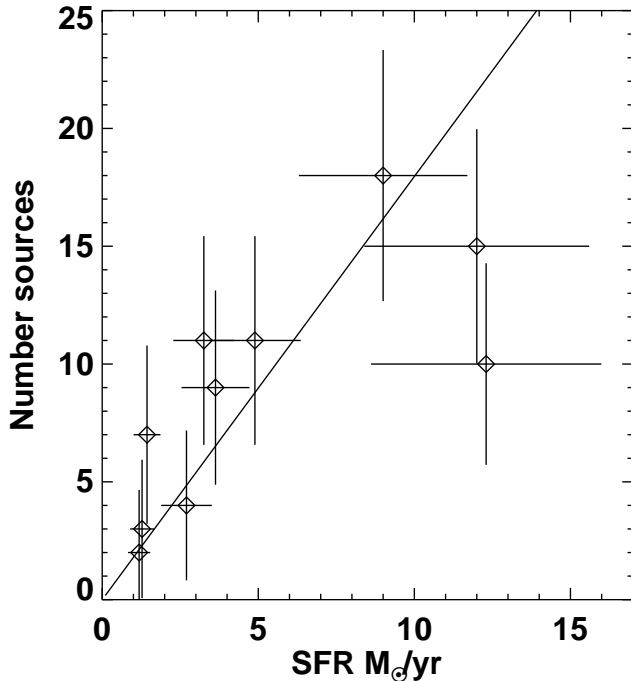


Fig. 5.— Number of point sources with luminosity above $2 \times 10^{38} \text{ erg s}^{-1}$ versus star formation rate for the galaxies listed in Table 5. The solid line is the linear fit described in the text.

the number of sources, N , with luminosities above $2 \times 10^{38} \text{ erg s}^{-1}$ and the total luminosity, L , of all point sources is $N = 4.9L/10^{40} \text{ erg s}^{-1}$. If the excess emission in the central region arises from point sources, then $N = 5.0^{+1.7}_{-1.2}$ sources would be expected. Using this estimate, the adjusted number of point sources in NGC 4194 would be 10. This is the number used in Table 5 and Fig. 5.

4. Relation of X-ray source population to star formation rate

Our primary goal is to extend the study of the relation between star formation rate and X-ray point source populations of galaxies to higher star formation rates (SFRs). NGC 7541 and NGC 4194 have SFRs significantly higher than any galaxy for which the X-ray point source population (as opposed to the total galactic X-ray luminosity) was studied by GGS03.

For NGC 4194, using the FIR luminosity versus SFR conversions adopted in GGS03 to calculate the SFR for stars more massive than $5M_{\odot}$ and cor-

recting for our assumed distance of 39.5 Mpc, we estimate a SFR of $9.1 M_{\odot} \text{ yr}^{-1}$ based on the far infrared (FIR) luminosity quoted by Buat et al. (2002), a rate of $12.6 M_{\odot} \text{ yr}^{-1}$ based on the FIR luminosity in Young et al. (1996), and a rate of $15.3 M_{\odot} \text{ yr}^{-1}$ based on the FIR luminosity in Deutsch & Willner (1987). The 1.4 GHz radio flux of NGC 4194 is 91.0 mJy when measured with a $1.5''$ beam (Condon et al. 1990), which gives a SFR of $30 M_{\odot} \text{ yr}^{-1}$ ($32.0 M_{\odot} \text{ yr}^{-1}$ for a $1.5''$ beam) using the relations in GGS03. The wide range of the SFR estimates for NGC 4194 highlight the difficulties with SFR estimation. Because we compare the X-ray luminosity directly with the FIR luminosity below, we adopt the mean, $12.3 M_{\odot} \text{ yr}^{-1}$, of the three FIR estimates as our best estimate of the SFR.

For NGC 7541, we estimate a SFR of $12.0 M_{\odot} \text{ yr}^{-1}$ based on the FIR luminosity in Young et al. (1996) calculated from the 60 and $100 \mu\text{m}$ fluxes, and a rate of $12.1 M_{\odot} \text{ yr}^{-1}$ based on the FIR luminosity calculated from the 12, 25, 60, and $100 \mu\text{m}$ fluxes from the IRAS survey using the formula in Deutsch & Willner (1987). We adopt the mean, $12.0 M_{\odot} \text{ yr}^{-1}$, of the two FIR estimates as our best estimate of the SFR.

Fig. 5 shows the relation between star formation rate and the number of X-ray point sources with luminosities above $2 \times 10^{38} \text{ erg s}^{-1}$ for the galaxies listed in Table 5. Fitting a linear relation to the data, we find a slope of $N(L > 2 \times 10^{38} \text{ erg s}^{-1}) = (1.8 \pm 0.4) \text{ SFR} / (M_{\odot} \text{ yr}^{-1})$. This fit was done considering the errors in both the SFR and the number of sources. The error on the SFR was taken as 30% of the SFR, for consistency with GGS03. The error on the number of sources was calculated using the method of Gehrels (1986). The fit has $\chi^2/\text{DoF} = 6.1/9$.

We note that our slope is lower than that quoted by GGS03. We expect that the number of sources found for each galaxy by GGS03 is higher than the true number for the following reasons. GGS03 did not correct the source luminosities quoted in the literature in various energy bands usually extending down to 0.5 or 0.1 keV to the 2-10 keV band used for the SFR versus X-ray luminosity relation. The GGS03 sample contained mainly nearby and large angular diameter galaxies, and, thus, would likely include a significant number of background AGN. These were not sub-

tracted out. The GGS03 sample may be biased to galaxies with unusually large X-ray point source populations, since the early *Chandra* observations of galaxies tended to be of those with high X-ray fluxes. Also, their sample contained many face-on galaxies. The source detection included counts in the soft X-ray band (usually down to 0.3 keV), and was, thus, most efficient for face-on galaxies where absorption within the host is low. This could be corrected by using only counts in the 2–10 keV for source detection. However, the relatively low effective area of *Chandra* above 2 keV would increase the detection threshold above $2 \times 10^{38} \text{ erg s}^{-1}$ in many cases. It is also possible that the difference reflects some dependence of X-ray source formation on the properties of the host galaxy.

The total X-ray luminosity has been suggested as a SFR indicator by Ranalli et al. (2003). We estimated the X-ray flux in the 2–10 keV band for each galaxy by summing the counts in the 2–8 keV band for all the point sources and then converting this sum to a total count rate and then to an unabsorbed energy flux assuming a power-law spectrum with a photon index $\Gamma = 1.7$ and given the absorption column density along the line of sight to the galaxy. For NGC 4194, we included all the counts in the larger nuclear region, but excluded the likely background AGN. We find a luminosity in the 2–10 keV band of $3.0 \times 10^{40} \text{ erg s}^{-1}$ for NGC 4194 and $1.8 \times 10^{40} \text{ erg s}^{-1}$ for NGC 7541. We note that both galaxies have sufficiently high SFR that they are in the linear regime of the L_X -SFR relation. The ratio of 2–10 keV luminosity, L_{40} , in units of $10^{40} \text{ erg s}^{-1}$, to SFR, in units of $M_\odot \text{ yr}^{-1}$, is $L_{40}/\text{SFR} = 0.24$ for NGC 4194 and 0.15 for NGC 7541. From the relation quoted above between SFR and the number of X-ray sources, and assuming the X-ray luminosity function of GGS03, we calculate a value of 0.37 ± 0.08 . This value is somewhat lower than, but not inconsistent with, the ratio of 0.5 found by Ranalli et al. (2003). Comparing directly with the FIR luminosity, we find $L_X = 1.6 \times 10^{-4} L_{\text{FIR}}$.

It is possible to estimate the fraction of mass involved in star formation which is accreted onto compact objects. We define $f = \dot{M}/\text{SFR}$, where $\dot{M} = L_X/(\eta c^2)$ and η is the efficiency for conversion of matter into radiation. If $\eta \sim 0.1$, then $f = (1.8 \times 10^{-6}) L_{40}/\text{SFR}$, where L_{40} is the luminosity in units of $10^{40} \text{ erg s}^{-1}$ and SFR

is the star formation rate in M_\odot/yr . Using the X-ray luminosity of SFR ratio found above, we find $f \sim 7 \times 10^{-7}$. Allowing a bolometric correction for the X-ray luminosity would increase this value by a factor of ~ 3 . This value should constrain population synthesis models of the formation and evolution of X-ray binaries. We note that this value includes only the ‘prompt’ accretion, i.e. that occurring while the star formation is still active. Additional accretion may occur, notably in the formation of low-mass X-ray binaries, well after active star formation has subsided.

Acknowledgments

We thank the anonymous referee for comments which helped improve the paper. PK acknowledges partial support from *Chandra* grant CXC GO4-7075X and STScI grant HST-GO-10769. This research has made use of the VizieR catalogue access tool, CDS, Strasbourg, France. This research has made use of the USNOFS Image and Catalogue Archive operated by the United States Naval Observatory, Flagstaff Station. This publication makes use of data products from the Two Micron All Sky Survey, which is a joint project of the University of Massachusetts and the Infrared Processing and Analysis Center/California Institute of Technology, funded by the National Aeronautics and Space Administration and the National Science Foundation.

REFERENCES

- Buat, V., Boselli, A., Gavazzi, G., Bonfanti, C. 2002, *A&A*, 383, 801
- Clark, D.M. et al. 2005, *ApJ*, 631, L109
- Condon, J.J., Helou, G., Sanders, D.B., Soifer, B.T. 1990, *ApJS*, 73, 359
- David, L.P., Jones, C., & Forman W. 1992, *ApJ*, 388, 82
- Deutsch, L.K. & Willner, S.P. 1987, *ApJS*, 63, 803
- Devereux, N.A. 1989, *ApJ*, 346, 126
- Dickey, J.M. & Lockman, F.J. 1990, *ARA&A*, 28, 215
- Eracleous, M., Shields, J.C., Chartas, G., Moran, E.C. 2002 *ApJ*, 565, 108

- Giacconi, R. 2001, 551, 624
- Gehrels, N. 1986, ApJ, 303, 336
- Griffiths, R.E. & Padovani, P. 1990, ApJ, 360, 483
- Griffiths, R.E., Ptak, A., Feigelson, E.D., Garmire, G., Townsley, L., Brandt, W.N., Sambruna, R., Bregman, J. N. 2000, Science, 290, 1325
- Grimm, H.-J., Gilfanov, M., & Sunyaev, R. 2003, MNRAS, 339, 793 – GGS03
- Hornschemeier, A.H. 2001, ApJ, 554, 742
- Ivo, S., Hibard, J.E., Rich, R.M. 2004, AJ, 127, 660
- Jha, S., Riess, A.G., Kirshner, R.P. 2007, ApJ, 659, 122
- Kaaret, P. 2001, ApJ, 560, 715
- Kilgard, R.E., Kaaret, P., Krauss, M.I., Prestwich, A.H., Raley, M.T., Zezas, A. 2002, ApJ, 573, 138
- Kilgard, R.E. et al. 2005, ApJS, 159, 214
- Koribalski, B. 1996, ASP Conf. 106, 238, ed. E.D. Skillman
- Monet, D.G. et al. 2003, AJ, 125, 984
- Ranalli, P., Comastri, A., & Setti, G. 2003, A&A, 399, 39
- Smith, D.A. & Wilson, A.S. 2003, ApJ, 591, 138
- Skrutskie, R.M. et al. 2006, AJ, 131, 1163
- Telesco, C.M., Becklin, E.E., Wynn-Williams, C.G., Harper, D.A. 1984, ApJ, 282, 427
- Terashima, Y. & Wilson, A.S. 2004, ApJ, 601, 735
- Weistrop, D., Eggers, D., Hancock, M., Nelson, C.H., Bachilla, R., Kaiser, M.E. 2004, AJ, 127, 1360
- Young, J.S., Allen, L., Kenney, J.D.P., Lesser, A., Rownd, B. 1996, AJ, 112, 1903

TABLE 6
X-RAY SOURCES WITHIN THE FIELD OF M100

#	RA	DEC	S/N	Counts	Flux (10^{-15} erg cm $^{-2}$ s $^{-1}$)	Luminosity (10^{38} erg s $^{-1}$)	Hardness	Counterpart
1	12 22 58.69	+15 47 51.8	65.0	169	37 ± 3	7.6	0.62	SN 1979C
2	12 22 54.78	+15 49 16.2	51.2	470	11 ± 5	21.6	0.66	C3
3	12 22 54.15	+15 49 12.3	42.6	203	46 ± 3	9.3	0.45	C2
4	12 22 49.12	+15 48 31.2	32.6	87	20 ± 2	4.1	0.79	
5	12 22 54.86	+15 49 18.1	28.2	205	46 ± 3	9.4	0.56	C1
6	12 22 50.40	+15 48 17.5	23.6	58	13.1 ± 1.7	2.7	0.78	
7	12 22 46.20	+15 48 49.6	20.0	55	13.2 ± 1.8	2.7	0.75	C6?
8	12 22 55.68	+15 49 24.9	16.3	88	23 ± 2	4.7	0.65	
9	12 22 58.24	+15 48 59.3	16.2	39	8.8 ± 1.4	1.8	0.69	
10	12 22 50.93	+15 50 42.7	14.9	46	16 ± 2	3.2	0.78	
11	12 22 58.38	+15 49 18.9	14.7	38	8.6 ± 1.4	1.8	0.87	
12	12 22 51.59	+15 49 37.7	14.7	35	28 ± 5	5.7	0.74	
13	12 22 54.25	+15 49 44.2	14.0	30	18.9 ± 3.5	3.8	0.67	C4
14	12 22 54.96	+15 49 20.1	13.9	104	23 ± 2	4.8	0.40	Nucleus
15	12 22 57.16	+15 48 57.4	12.6	30	6.8 ± 1.2	1.4	0.57	
16	12 22 43.76	+15 51 01.9	11.8	47	17 ± 3	3.5	0.91	
17	12 22 43.22	+15 51 04.7	11.6	46	17 ± 3	3.5	0.70	SDSS
18	12 22 44.54	+15 49 28.0	11.5	27	15 ± 3	3.0	0.78	
19	12 23 00.87	+15 46 38.4	11.0	24	5.3 ± 1.1	1.1	0.33	2mass
20	12 22 50.83	+15 47 01.4	10.3	24	5.4 ± 1.1	1.1	0.88	
21	12 22 51.11	+15 48 59.5	8.9	26	5.9 ± 1.2	1.2	0.69	
22	12 22 54.52	+15 49 04.4	8.5	31	7.0 ± 1.3	1.4	0.65	
23	12 22 47.11	+15 49 13.1	8.0	24	5.7 ± 1.2	1.2	0.88	
24	12 22 55.99	+15 48 41.3	7.6	18	4.0 ± 0.9	0.8	0.89	
25	12 22 58.40	+15 47 26.5	7.4	17	3.9 ± 1.0	0.8	0.71	
26	12 22 52.06	+15 47 14.6	6.3	16	3.6 ± 0.9	0.7	0.88	
27	12 22 54.73	+15 48 03.6	6.2	15	3.3 ± 0.9	0.7	1.00	
28	12 22 55.97	+15 49 09.9	6.1	22	5.0 ± 1.1	1.0	0.68	
29	12 22 56.83	+15 46 30.9	5.9	15	3.3 ± 0.9	0.7	0.80	
30	12 23 01.97	+15 51 33.1	5.5	15	5.0 ± 1.3	1.0	0.73	
31	12 22 57.39	+15 48 19.8	5.4	13	2.9 ± 0.8	0.6	0.69	[FFH96] C64?
32	12 22 52.23	+15 48 59.9	5.1	13	2.9 ± 0.8	0.6	0.69	
33	12 22 50.00	+15 48 28.2	5.1	16	3.6 ± 0.9	0.7	0.44	
34	12 22 49.75	+15 51 30.9	4.8	11	3.8 ± 1.1	0.8	0.73	
35	12 22 49.70	+15 47 43.7	4.4	10	2.3 ± 0.7	0.5	0.80	
36	12 22 57.71	+15 49 36.5	4.2	9	5.0 ± 1.7	1.0	0.67	
37	12 22 45.94	+15 47 16.6	4.1	11	2.8 ± 0.8	0.6	0.73	
38	12 22 53.06	+15 48 33.4	4.1	10	2.2 ± 0.7	0.5	0.60	
39	12 23 05.67	+15 48 53.1	4.1	9	2.0 ± 0.7	0.4	1.00	
40	12 22 51.06	+15 49 47.6	4.0	10	3.5 ± 1.1	0.7	0.70	
41	12 22 57.65	+15 48 39.4	3.9	9	2.0 ± 0.7	0.4	0.33	
42	12 22 57.54	+15 48 16.5	3.7	9	2.0 ± 0.7	0.4	0.89	
43	12 22 54.89	+15 50 16.7	3.6	8	2.6 ± 0.9	0.5	0.62	
44	12 22 54.49	+15 50 15.4	3.6	8	2.6 ± 0.9	0.5	0.12	
45	12 23 03.02	+15 48 27.0	3.6	8	1.8 ± 0.6	0.4	1.00	
46	12 22 52.68	+15 48 36.2	3.4	9	2.0 ± 0.7	0.4	0.44	
47	12 22 48.08	+15 50 53.5	3.3	8	2.7 ± 1.0	0.6	0.50	
48	12 22 55.42	+15 49 16.8	3.2	39	8.8 ± 1.4	1.8	0.31	2mass
49	12 22 53.23	+15 48 32.2	3.1	7	1.6 ± 0.6	0.3	0.43	
50	12 23 05.62	+15 50 44.5	3.0	6	2.0 ± 0.8	0.4	0.50	

NOTE.—The quantities are as defined for Table 2. Counterparts C1-C6 indicate sources from Kaaret (2001).

TABLE 7
X-RAY SOURCES WITHIN THE FIELD OF NGC 4945

#	RA	DEC	S/N	Counts	Flux (10^{-15} erg cm $^{-2}$ s $^{-1}$)	Luminosity (10^{38} erg s $^{-1}$)	Hardness	Counterpart
1	13 05 21.95	-49 28 26.6	389.5	1349	466 \pm 13	5.0	0.89	
2	13 05 32.88	-49 27 34.1	358.5	1311	439 \pm 12	4.7	0.93	
3	13 05 38.10	-49 25 45.5	232.4	705	328 \pm 12	3.5	0.91	
4	13 05 18.54	-49 28 24.0	189.0	496	172 \pm 8	1.85	0.82	
5	13 05 35.49	-49 29 11.4	139.7	340	118 \pm 6	1.27	0.82	
6	13 05 34.61	-49 27 51.8	124.9	297	99 \pm 6	1.06	0.92	
7	13 05 27.49	-49 28 05.2	86.6	341	121 \pm 7	1.29	1.00	
8	13 05 22.25	-49 29 12.5	86.5	223	76 \pm 5	0.8	0.66	
9	13 05 22.86	-49 29 01.4	74.5	197	67 \pm 5	0.7	0.96	
10	13 05 25.47	-49 28 32.4	70.4	194	66 \pm 5	0.7	0.98	
11	13 05 40.78	-49 26 03.6	62.5	115	54 \pm 5	0.6	0.99	
12	13 05 21.18	-49 27 41.3	58.0	157	59 \pm 5	0.6	0.82	
13	13 05 28.96	-49 29 44.3	57.7	133	46 \pm 4	0.5	0.86	
14	13 05 16.36	-49 27 34.8	54.3	128	44 \pm 4	0.5	0.80	
15	13 05 21.69	-49 27 37.0	49.6	130	46 \pm 4	0.5	0.77	
16	13 04 42.57	-49 34 49.5	44.4	350	196 \pm 10	2.1	0.96	
17	13 05 22.40	-49 26 57.5	41.1	95	32 \pm 3	0.3	0.87	
18	13 05 22.51	-49 29 35.3	40.1	88	31 \pm 3	0.3	0.93	
19	13 05 24.35	-49 27 21.8	29.0	59	20 \pm 3	0.2	0.78	
20	13 05 28.95	-49 27 05.2	25.0	54	18 \pm 2	0.2	0.91	
21	13 05 22.79	-49 28 52.9	22.2	40	14 \pm 2	0.15	0.98	
22	13 05 22.67	-49 27 53.0	21.9	48	16 \pm 2	0.18	0.96	
23	13 05 27.11	-49 28 04.4	19.4	73	26 \pm 3	0.3	0.95	
24	13 05 11.04	-49 31 26.1	18.3	62	22 \pm 3	0.2	0.39	
25	13 05 29.79	-49 26 43.1	16.2	31	10 \pm 2	0.11	0.81	
26	13 05 09.79	-49 31 42.8	16.0	62	21 \pm 3	0.2	0.95	
27	13 05 37.23	-49 26 02.0	15.0	29	13 \pm 2	0.14	0.86	
28	13 05 25.42	-49 28 24.0	13.1	33	11 \pm 2	0.12	1.00	
29	13 05 13.26	-49 28 33.7	10.9	24	8.7 \pm 1.7	0.09	0.75	
30	13 05 43.39	-49 24 31.4	8.8	20	10 \pm 2	0.11	0.95	
31	13 05 35.49	-49 25 27.0	8.4	16	7.5 \pm 1.9	0.08	1.00	
32	13 05 26.65	-49 27 41.9	7.0	21	7.1 \pm 1.5	0.08	0.62	
33	13 04 56.68	-49 33 40.2	6.2	33	17 \pm 3	0.18	0.82	
34	13 05 30.01	-49 28 20.2	5.9	13	4.5 \pm 1.3	0.05	0.85	
35	13 05 24.91	-49 28 39.9	5.3	11	3.8 \pm 1.1	0.04	1.00	
36	13 05 39.10	-49 25 29.7	5.1	11	5.1 \pm 1.6	0.06	0.82	
37	13 05 11.13	-49 29 02.5	4.9	10	3.5 \pm 1.1	0.04	1.00	
38	13 05 33.16	-49 27 01.4	4.9	9	3.0 \pm 1.0	0.03	0.44	
39	13 05 27.47	-49 29 30.8	4.9	10	3.5 \pm 1.1	0.04	1.00	
40	13 05 31.19	-49 27 49.0	4.6	10	3.4 \pm 1.1	0.04	0.90	
41	13 05 31.78	-49 26 58.2	4.4	10	3.4 \pm 1.1	0.04	0.80	
42	13 05 35.63	-49 26 58.8	4.2	7	2.4 \pm 0.9	0.03	1.00	
43	13 05 23.14	-49 27 54.9	4.1	11	3.7 \pm 1.1	0.04	0.73	
44	13 05 36.70	-49 27 22.1	4.0	9	3.0 \pm 1.0	0.03	1.00	
45	13 05 14.92	-49 30 42.5	3.8	12	4.0 \pm 1.2	0.04	0.50	
46	13 05 52.86	-49 23 12.2	3.7	11	5.5 \pm 1.7	0.06	0.45	
47	13 05 42.95	-49 25 09.1	3.6	7	3.3 \pm 1.3	0.04	1.00	
48	13 05 19.53	-49 30 03.2	3.0	5	1.7 \pm 0.8	0.02	0.60	

NOTE.—The quantities are as defined for Table 2.